ACS OMEGA

Open Access

http://pubs.acs.org/journal/acsodf

Article

In Vitro Hemoglobin Binding and Molecular Docking of Synthesized Chitosan-Based Drug-Carrying Nanocomposite for Ciprofloxacin-HCl Drug Delivery System

Yahiya Kadaf Manea,* Mohsen T. A. Qashqoosh, and Mashallah Rezakazemi*

Cite This: *ACS Omega* 2024, 9, 6339−6354

Read Online

ACCESS | Metrics & More | Article Recommendations | Supporting Information

ABSTRACT: Understanding the intermolecular interactions between antibiotic drugs and hemoglobin is crucial in biological systems. The current study aimed to investigate the preparation of chitosan/polysorbate-80/tripolyphosphate (CS-PS/TPP) nanocomposite as a potential drug carrier for Ciprofloxacin-HCl drug (CFX), intended for controlled release formulation and further used to interact with bovine hemoglobin. Fourier transform infrared (FT-IR) spectroscopy, thermogravimetric analysis−differential thermal analysis (TGA-DTA), scanning electron microscopy (SEM), dynamic light scattering (DLS), and X-ray diffraction analyses were used to characterize the CS-PS/TPP nanocomposite and its CFX-loaded nanocomposite. The second series of biophysical properties were performed on the Ciprofloxacin-loaded CS-PS/TPP (NCFX) for interaction with bovine hemoglobin (BHb). The interactions of (CFX and NCFX) with redox protein hemoglobin were investigated for the first time through a series of in vitro experimental techniques to provide comprehensive knowledge of the drug−protein binding interactions. Additionally, the effect of inclusion of PS-80 on the CFX-BHb interaction was also studied at different concentrations using fluorescence spectroscopy, ultraviolet−visible (UV−Vis) spectroscopy, and circular dichroism (CD) under physiological conditions. The binding process of CFX and NCFX was spontaneous, and the fluorescence of BHb was quenched due to the static mechanism formation of the (CFX/BHb) and (NCFX/BHb) complexes. Thermodynamic parameters ΔG, ΔH, and ΔS at various temperatures indicate that the hydrogen bonding and van der Waals forces play a major role in the CFX-BHb association.

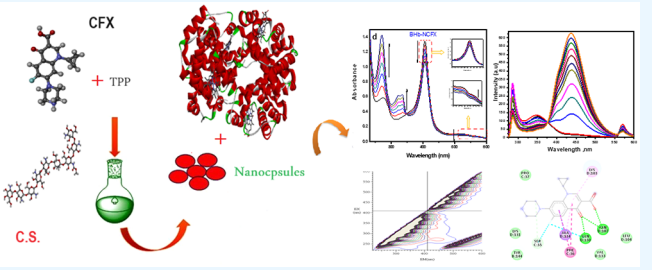

1. INTRODUCTION

In recent years, the development of new drug delivery systems has received considerable attention from researchers to overcome deficiencies in traditional pharmaceutical components aiming to achieve patient compliance and clinical efficacy.[1] Polysaccharides-based natural polymers are suitable for drug applications due to their biocompatibility, biodegradability, and low immunogenicity.[2] The development of biopolymer-based nanocomposites used as base materials in pharmaceutical applications is necessary to achieve the controlled release of therapeutics excellently.[3,4] Most antibiotic drugs are hydrophobic, and delivering them effectively to their target is a huge challenge. Further, studies on the interaction between antibiotic drugs and biological macromolecules could improve the understanding of the absorption, transportation,[5,6] distribution, metabolism behaviors, and possible mechanism of these drugs, thereby helpful in designing, improving, and modifying drug molecules.[7] Human hemoglobin (Hb) is a protein known for the transport of oxygen (O_2) from the lungs to different respiring tissues.[8] Structurally, this molecule contains two (α-globin) and two (β-globin) subunits, noncovalently associated with erythrocytes as a tetramer; each α-chain contains 141 amino acid residues and each β-chain includes 146 amino acid residues. Hb can reversibly bind several endogenous and exogenous molecules and thus act as a drug carrier for effective delivery to the required physiological site for drug therapy in treating diseases. Therefore, knowledge of the binding characteristics of these therapeutically important antibiotics with Hb is critical for understanding their possible use in delivery and consequent availability in the required tissues. Bovine hemoglobin (BHb) has been reported as a model protein that is 90% homologous to human hemoglobin concerning amino acid sequence, a better oxygen carrier, and less exothermic oxygen binding capacity.[9] It has already been confirmed that antibiotic compounds can form strong intermolecular complexes with proteins; therefore, this work investigates how to minimize the amount of ciprofloxacin by using it in nano form. Ciprofloxacin (CFX) drug in its nano form could be used effectively to escape the side effects of accumulation due to use. On the other hand, hemoglobin (BHb)

Received: June 28, 2023
Revised: December 27, 2023
Accepted: December 28, 2023
Published: January 31, 2024

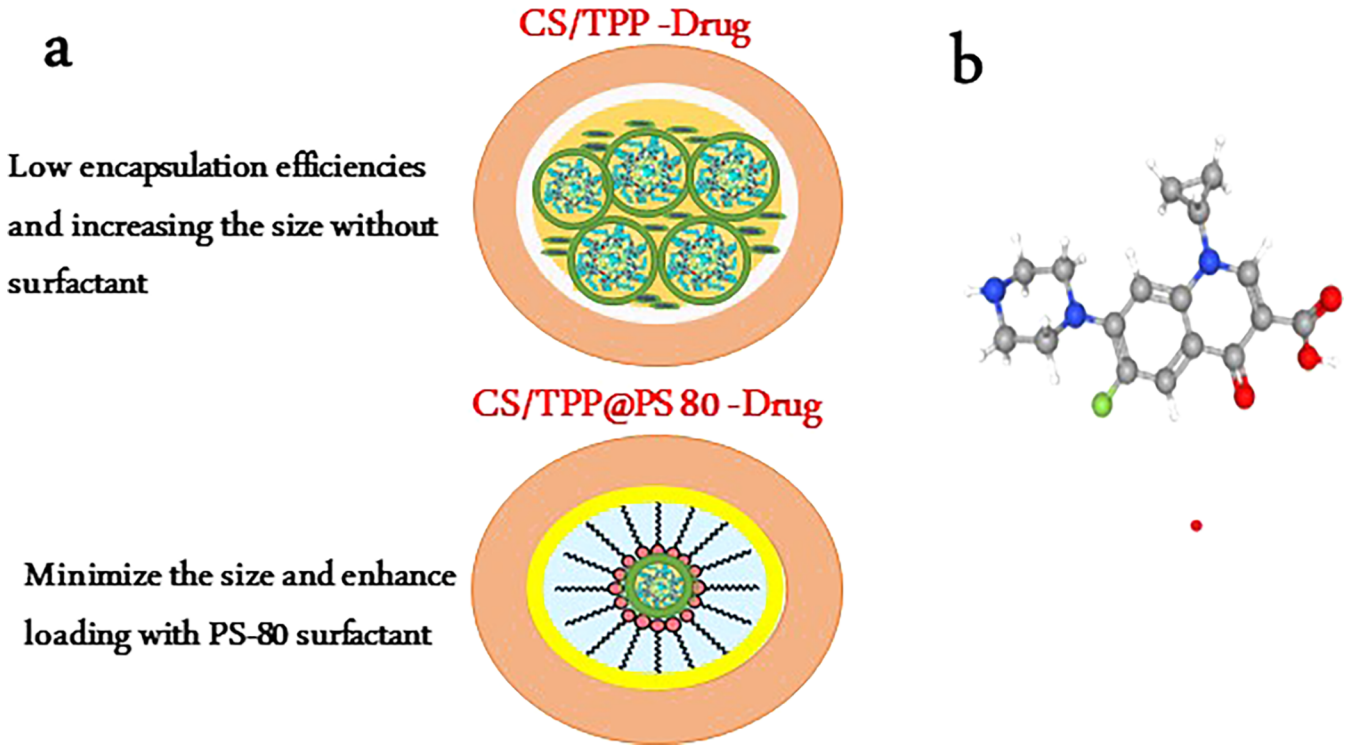

Figure 1. (a) Scheme representing the encapsulation routes of CFX in the presence and absence of PS-80. (b) Molecular structure of a ciprofloxacin−HCl.

serves as a carrier molecule for multiple drugs and the interaction of CFX/NCFX with BHb is not characterized so far. Consequently, the investigation of transport processes in ciprofloxacin−protein system is highly significant in the pharmacological field.[10,11] The hydrophobic interaction of nonionic surfactants with proteins has been considered as one of the key factors for preventing aggregation and the agitation-induced denaturation of proteins during biotechnological processes.[12] Hemoglobin molecules can also act as binders for drugs. The interaction studies of bovine hemoglobin with antibiotics drugs,[13] flavonoids[14] heteropolyacids,[15,16] artemisinins,[17] herbicides, surfactants, hematoporphyrins,[18] and insecticides have been reported. However, the interaction of CFX and NCFX with BHb has not been investigated, especially the effect of the polysorbate-80 surfactant on the binding of drugs to BHb. Protein surfactant-based interactions are remarkably dependent on the surfactants' features (functional groups). It is a well-observed binding of surfactants with proteins that may induce either stabilization or denaturation of the protein structure. Surfactants also affect protein aggregation, sometimes perturbating proteins' biological functions.[19,20] In this regard, the present work deals with the effect of surfactant (PS-80) upon loading CFX drug into chitosan/tripolyphosphate (CS-TPP) nanocomposite to evaluate the interaction binding of drug released with BHb. The surfactant PS-80 helps in the controlled release of NCFX. Therefore, more amount of NCFX is freely released, which is available to the targeted tissues as compared to CFX released from plasma. This facilitates NCFX to deliver its optimum medicinal effects in tiny amounts. In addition, the physicochemical parameters of an encapsulated drug, such as molecular docking, quenching constants, binding constants, and number of binding sites, were discussed (Figure 1).

2. EXPERIMENTAL SECTION

2.1. Materials and Methods. Bovine hemoglobin (BHb) (ref number: H2500, lyophilized powder) was supplied from Sigma and was used as such. Ciprofloxacin−HCl standard was supplied from Cipla Ltd., India. Tripolyphosphate (TPP), chitosan (C.S.) with a low deacetylation degree, DD: 81% and high molecular weight, M_W: 425 kDa, and Polysorbate-80 (P.S.) were supplied from (Merck. Co., India). The concentration of hemoglobin has been fixed at 10 μM during this study.[21] All other reagents used were of analytical grade. Deionized water was used in the entire experiment.

The chitosan nanocapsules (C.S./PS-TPP) were developed through ionotropic gelation of chitosan with PS/TPP. Different concentrations of chitosan (0.5−1%) were dissolved in 100 mL of 2% v/v acetic acid. Tripolyphosphate (TPP) solution (0.5%) was prepared by adding 500 mg of TPP in 100 mL of 5% (polysorbate−80) to prevent particle aggregation. Individually, 15 mg of CFX dissolved in deionized water was added into the PS-80/TPP mixture and placed in the ultrasonic bath for 1 h. Finally, the PS-80/TPP@CFX mixture was added dropwise into C.S. solution and stirred for 3 h on the homogenizer. The C.S./PS-TPP@CFX nanocapsule production started spontaneously via the ionic gelation mechanism. The C.S./PS-TPP@CFX nanocapsules were kept overnight in the dark to homogenate, then centrifuged at 10,000 for 20 min, and freeze-dried before further analysis.[22]

2.2. Drug Entrapment Efficiency. The suspensions of CFX-loaded C.S./PS-TPP were centrifuged at 5000 rpm for 20 min, and the supernatant liquid was determined spectrophotometrically, allowing the determination of the drug entrapment efficiency.[23] The drug entrapment efficiency (DEE %) was estimated using the following equation:

https://doi.org/10.1021/acsomega.3c04632
ACS Omega 2024, 9, 6339−6354

$$\text{DEE}\ (\%) = \frac{\text{amount of drug actually present}\ (\mu g)}{\text{theoretical drug load expected}} \times 100 \quad (1)$$

All analyses were performed in triplicate measurements. All measurements were investigated with a double beam (R Beam Att, S Beam Att, 60 mm sphere) in the 200−800 nm wavelength range at 25 °C.

2.3. Drug Release. The nanocomposite loaded drug suspension was prepared by taking 25 mg of CFX@CS/PS-TPP nanocomposite and placing it in 25 mL of phosphate-buffered saline (PBS) with various pH values on sink conditions. The entire system was kept at 25 °C while being shaken in an incubator for 2 days. The amount of Ciprofloxacin released from the nanocomposite (NCFX) was analyzed by UV−Vis measurement. The % drug release (NCFX) was determined by the following equation:[24]

$$\text{drug release}\ \% = \frac{C_t}{C_0} \times 100 \quad (2)$$

To evaluate the accumulative release of NCFX drug, the solution (1 mL) was extracted at different time intervals, and fresh PBS (1 mL) was added to the release solution for continuing incubation. The NCFX release experiments were repeated three times.

2.4. Quenching Constant. The interactions of NCFX, CFX, CFX−PS_1, and CFX-PS_2 with BHb were studied using fluorescence spectroscopy with varied concentrations of drug from 0.5 to 5.0 × 10^{-5} M. The quenching mechanisms were analyzed by the well-known Stern−Volmer equation

$$\frac{F_0}{F} = 1 + K_{SV}[Q] = 1 + k_q\tau_0[Q] \quad (3)$$

where F_0 and F denote the steady-state fluorescence intensities in the absence and presence of a quencher (CFX), respectively, K_{SV} is the Stern−Volmer quenching constant, and [Q] is the concentration of the quencher regression of a plot of F_0/F against [Q].[25]

Fluorescence spectra were recorded by exciting the hemoglobin solution at 280 nm and keeping excitation and emission slit widths at 5 nm each. Scans were performed in the 220−650 nm range at a rate scan of 1500 nm min^{-1}. All experimental results of fluorescence intensities for ligand and BHb were studied by using the equation of the inner filter correction as follows:

$$F_{corrected} = F_{observed} D 10^{(A_{280}+A_{340})/2} \quad (4)$$

where $F_{corrected}$ and $F_{observed}$ are the corrected and observed fluorescence intensities, respectively; D is the dilution factor; and A_{280} nm and A_{340} nm are the sum of the absorbance of BHb and ligand at the excitation 280 nm and emission (340 nm) wavelengths, respectively.[26,27]

2.5. Binding Constant. The usefulness of the drugs in the biological system is essentially subjected to their binding ability, which can also impact the drug stability and toxicity during their chemotherapeutic process. In addition, the drug−protein complex may be considered an excellent miniature model for gaining insights into the general drug−protein interaction. The fluorescence intensity data determined the binding constant values to calculate the binding interaction between CFX@CS/PS-TPP nanocomposite, PS1-CFX, PS2-CFX, and CFX pure with hemoglobin. When small molecules bind independently to the asset of equivalent sites on a macromolecule, the equilibrium between free and bound molecules is given by the following equation:

$$\log\left[\frac{F_0 - F}{F}\right] = \log K_A + n \log[Q] \quad (5)$$

where (K_A) is the binding constant used to calculate the standard free energy change ΔG^0 of the drug binding to BHb from the relationship in eq 3.[28] The interaction between biomacromolecules and drugs is categorized into four types of bonding forces: hydrogen bonds, electrostatic, weak Van der Waals, and hydrophobic, which can be evaluated using the thermodynamic parameters via enthalpy change (ΔH), free energy change (ΔG), and entropy change (ΔS). These parameters can be calculated using Van't Hoff thermodynamic equations.

$$\log K = -\frac{\Delta H^\circ}{2.303RT} + \frac{\Delta S^\circ}{2.303R} \quad (6)$$

$$\Delta G^\circ = -RT \ln K_A = \Delta H^\circ - T\Delta S^\circ \quad (7)$$

where K_A is the binding constant at the corresponding temperature T (K) and R (1.987 cal K^{-1} mol) is the gas constant.[29] The negative value of ΔG reveals that the interaction proceeds spontaneously in the standard state.

2.6. Synchronous Spectroscopy. Synchronous spectra of BHb with CFX, NCFX, and CFX/PS in different concentrations at 298 K were studied, and the wavelength difference ($\Delta\lambda$) between excitation wavelength (λ_{ex}) and emission wavelength (λ_{em}) was fixed at 15 and 60 nm, respectively, in the wavelength range 200−500 nm.

2.7. Energy Transfer to CFX and NCFX. The energy (E) transfer between (CFX and NCFX) and BHb was studied by scanning the fluorescence spectra of BHb and absorption spectra of CFX and NCFX in the wavelength range between 250 and 450 nm at 25 °C. According to Forster's theory, the efficiency of energy transfer (E) is calculated using the following equation:[30]

$$E = 1 - \frac{F}{F_0} = \frac{R_0^6}{R_0^6 + r^6} \quad (8)$$

where F_0 and F are the fluorescence intensities of BHb in the absence and presence of drug, respectively, r is the distance between the donor and the acceptor molecules, and R_0 is the critical distance for 50% transfer efficiency, which can be calculated by the following equation:

$$R_0{}^6 = 8.8 \times 10^{-25} k^2 n^{-4} \Phi J \quad (9)$$

where k^2 is the spatial orientation factor of the dipole, $k^2 = 2/3$; n is the refractive index of the medium, n = 1.36; Φ is the fluorescence quantum yield of the donor, Φ = 0.062 for BHb;[31] and J is the overlap integral of the emission spectrum of the donor and the absorption spectrum of the acceptor, which can be calculated by the following equation:

$$J = \frac{\sum F(\lambda)\varepsilon(\lambda)\lambda^4\Delta\lambda}{\sum F(\lambda)\Delta\lambda} \quad (10)$$

where $F(\lambda)$ is the fluorescence intensity of the fluorescence donor at wavelength λ and $\varepsilon(\lambda)$ is the molar absorption coefficient of the acceptor at this wavelength. The absorption spectra were obtained at a constant BHb concentration (5 μM) and varying CFX and NCFX concentrations from 0 to 3.5 μM.

https://doi.org/10.1021/acsomega.3c04632
ACS Omega 2024, 9, 6339−6354

Table 1. Conditions of Synthesis for Various Concentrations of Chitosan/PS-TPP Nanocomposites

s.no.	sample-I	sample-II	sample-III	sample-IV	sample-V	sample-VI
CS (g/L)	0.50	0.50	0.50	0.75	1.00	0.5
polysorbate-80 (5%) %v/v	10	20	50	10	10	
TPP (g/L)	0.45	0.40	0.25	0.45	0.45	0.50
CFX loaded (0.15 g/L)	59.4%	49.8%	45.7%	44.7%	47.3%	34.9%

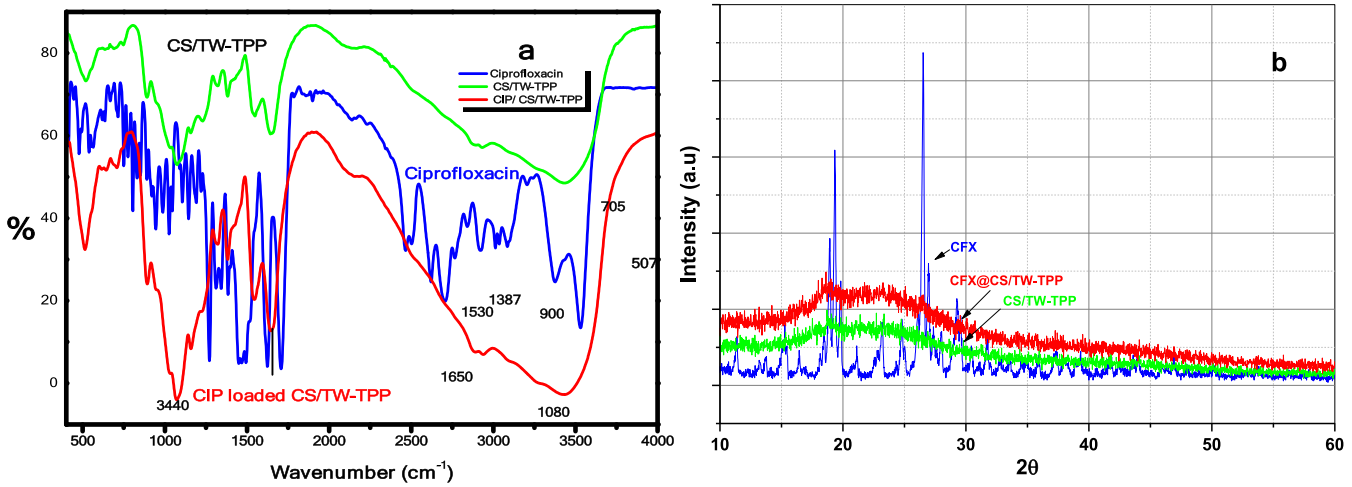

Figure 2. (a) FT-IR spectra of CFX, CFX@CS/PS-TPP, and CS/PS-TPP; (b) XRD patterns of CFX and CS/PS-TPP before and after loading of CFX

2.8. Circular Dichroism (CD). The influence of Ciprofloxacin on the secondary structure of BHb was performed using circular dichroism spectroscopy in varied molar ratios of drug to protein (0, 1:1, and 2:1) at room temperature. Circular dichroism spectral results are quantitatively analyzed by calculating the % α-helicity using the following relationships. The mean residue ellipticity (MRE) is given as follows:

$$\text{MRE (deg cm}^{-1}\text{ dmol}^{-1}) = \frac{\text{observed CD (mdeg)}}{nl \times [C_p] \times 10} \quad (11)$$

$$\alpha\text{-helix (\%)} = \frac{-(\text{MRE}_{222} - 3000)}{36\,000 - 3000} \times 100 \quad (12)$$

where the observed CD indicates ellipticity at 222 nm, L is the optical path length (here l = 0.1 cm), and n is the number of amino acid residues in the protein for BHb n = 574.

2.9. Docking Studies. The docking studies have been investigated by employing AutoDock 4.2 Vina software and AutoDock Tools (ADT) using the Lamarckian genetic algorithm. The crystal structure of BHb (PDB ID: 1G09) was downloaded from Brookhaven Protein Data Bank, and the three-dimensional structure of CFX (CID = 2764) was retrieved from PubChem. During the preparation of protein files with AutoDock Tools, polar hydrogens and Kollman charges were assigned. The AutoDock run utilized the following parameters: G.A. population size, 150; maximum energy evolutions, 2.5 × 10^6. Grid box size 90 Å × 90 Å × 90 Å along x, y, and z axes covering whole protein with a grid-point spacing of 0.708 Å were assigned. For visualization and identification of the residues involved, Discovery Studio 3.5 was utilized. Different site-specific probes, Warfarin for site I and ibuprofen for site II, were utilized for performing displacement studies.

3. RESULTS AND DISCUSSION

The current study tried to mimic the in vivo conditions, such as physiological hemoglobin concentrations, buffer, blood pH value, and human body temperature. During this experiment, the value of pH was kept constant at 7.4 using phosphate buffer; this value is similar to the pH value of blood. Finally, CFX, CFX-PS1, CFX-PS2, and NCFX were mixed individually with BHb at body temperatures of 25−37 °C. Therefore, the experimental conditions are close to the conditions in vivo. The conditions of synthesis for various concentrations of chitosan/PS-TPP nanocomposites in the presence and absence of CFX drug are presented in Table 1. The addition of surfactant polysorbate-80 (P.S.)5% into the chitosan/TPP system enhanced the stability and loading efficiency and reduced the size of nanoparticles. Polysorbate-80 surfactant is well known for its hydrophilic nature and would interact strongly with chitosan molecules. Chin et al. found that the presence of surfactants during the precipitation process could have limited the growth of chitosan nanoparticles, and thus the observed particles of reduced mean sizes.[32] The in vitro drug release study was conducted on all preparations (2, 4, 6, 8, and 10% drug-loaded samples). The optimum ratio containing chitosan/PS/TPP (1:0.1:0.9) was selected for drug loading.

3.1. FT-IR, XRD, and Thermal Stability. The peak values of FT-IR analysis, which confirmed the presence of functional groups of chitosan, TPP, polysorbate-80, and CFX are shown in Figure 2a. Chitosan peak values were characterized with specific peaks at 1643, 903, and 3456 cm^{-1}, which may be singed to function groups of amide (CO−NH_2), anhydro glucosidic ring, and primary amine (−NH_2), respectively. From the intensity peaks of the nanocomposite, the observed peaks at 1643 and 3456 cm^{-1} show a slightly shifted to lower-wavenumber region at 1636 and 3410 cm^{-1}. The reduction in stretching frequency could be attributed to the TPP interaction with the ammonium group of chitosan and more hydrogen bonding in the CFX@CS/PS−TPP complex.[33]

https://doi.org/10.1021/acsomega.3c04632
ACS Omega 2024, 9, 6339−6354

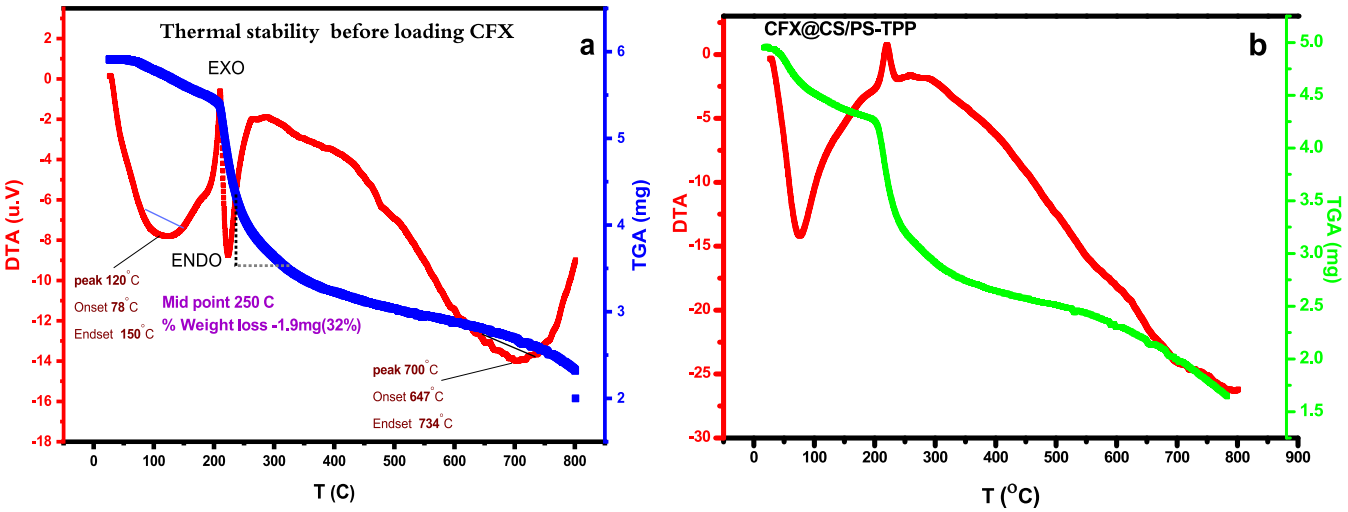

Figure 3. (a) TGA-DTA studies of CS/PS-TPP. (b) TGA-DTA analysis of CFX@CS/PS-TPP

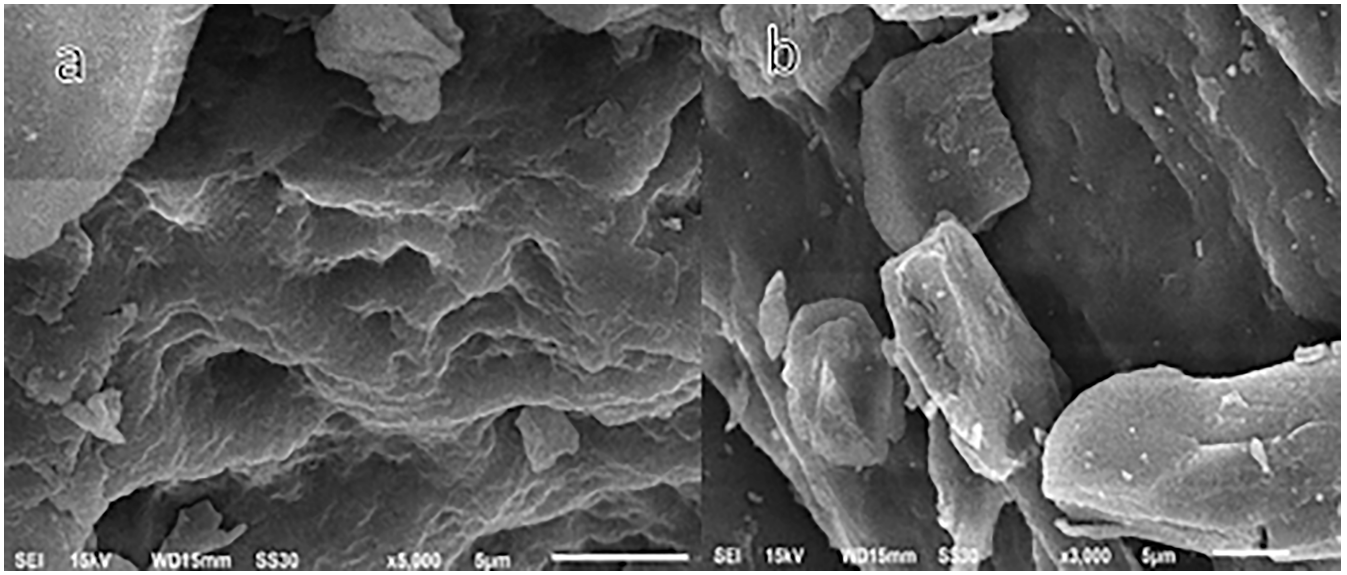

Figure 4. SEM images of CS/PS-TPP before (a) and after (b) loading with CFX.

Figure 2b shows the wide-angle X-ray diffractograms of CS/PS-TPP, Ciprofloxacin (CFX), and the CFX@CS/PS-TPP nanocomposite. To ensure the availability of CFX on CS/PS-TPP, XRD was recorded under identical conditions for CS/PS-TPP and CFX@CS/PS-TPP to confirm the loading of Ciprofloxacin. The XRD pattern of the CS/PS-TPP has a broad peak centered at 19.46° which is attributed to the presence of the two components C.S. and TPP, while two small peaks at (25 and 28°) may be due to the loading of drug into chitosan capsule.

The thermal decomposition (TGA) and (DTA) characteristics of CS/PS-TPP and CFX@PS-TPP are shown in Figure 3a,b respectively. Weight loss was observed when the composite was heated from room temperature to 200 °C. This region is related to water and organic species evaporation, which is associated with weight loss of about 16 and 26% for CS/PS-TPP and CFX @ CS/PS-TPP, respectively.[34] The composites were shown to be thermally stable at lower than 200 °C due to intermolecular spaces between the chitosan chain and P.S. and TPP, which subsequently decreased the H-bond interactions between the chains as suggested by Martins et al.[35] The increase of temperature in the region 210−500 °C shows continuous decomposition of CS/PS-TPP and CFX@CS/PS−TPP accompanied with weight loss 50 and 36.73% for CS/PS-TPP and CFX-loaded CS/PS-TPP, respectively, attributed to the degradation and deacetylation of chitosan.[36] The activation energy (E_a) of CFX @CS/PS-TPP and CS/PS-TPP were estimated using the method of Broido.[37,38] The values indicated that the activation energy value increased by loading of CFX from 17.4 to 24.5 (kJ mol^{-1}) due to an increase in the broken bonds between the CFX − CS/PS-TPP composite. The results of DTA curves were supported by TGA. The DTA curve of CS/PS-TPP showed an endothermic peak with a maximum at 200 °C due to dehydration reaction, while in the case of CFX@CS/PS-TPP composite, an exothermic broad peak occurred at 200 °C due to the encapsulation of CFX.

3.2. Morphology and Particle Size Analysis. Scanning electron microscopy was carried out to evaluate the surface morphology of CS/PS-TPP nanocomposite before loading the drug (Figure 4a) and after loading (Figure 4b), which displayed a spherical-shaped nanocomposite material. Dynamic light scattering (DLS) diagrams of nanomaterials obtained from

https://doi.org/10.1021/acsomega.3c04632
ACS Omega 2024, 9, 6339−6354

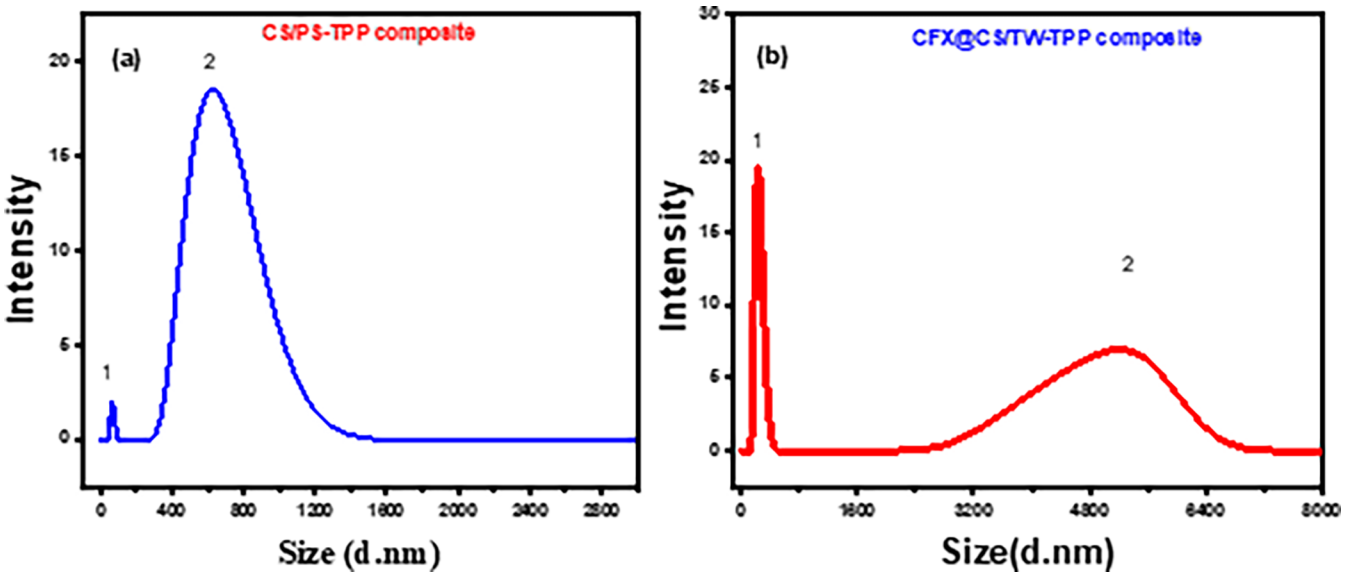

Figure 5. (DLS) Particle size distribution curves of CS/PS-TPP before (a) and after (b) loading with ciprofloxacin.

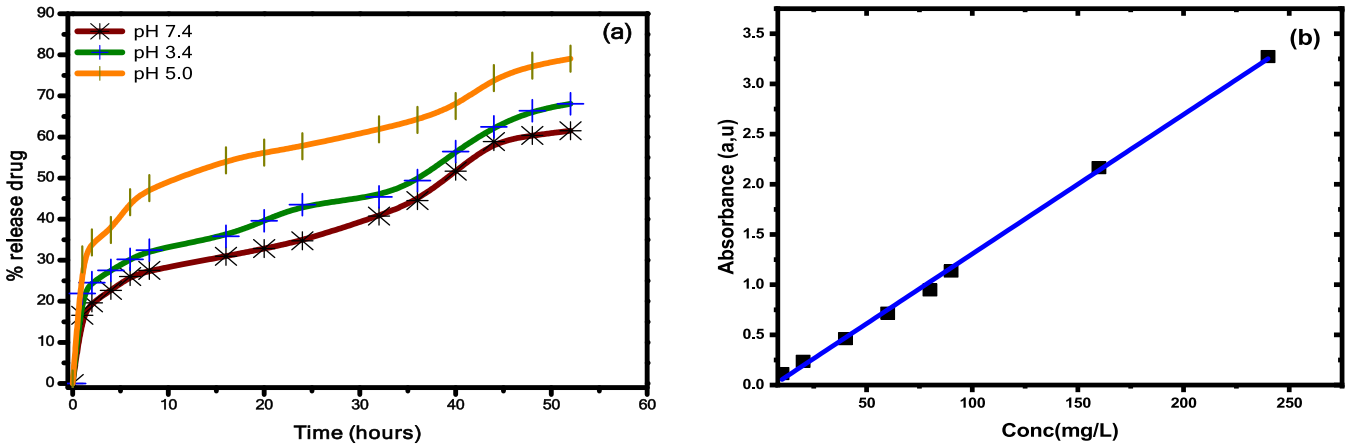

Figure 6. Release profiles of CFX from CS/PS-TPP nanocomposite at various pH values (a). Calibration curve of CFX from CS/PS-TPP nanocomposite at 298 K (b).

CS-PS/TPP and CFX-loaded CS-PS/TPP, respectively, are shown in Figure 5a,b. The differences in the size of particles at peaks 1 and 2 for CS/PS-TPP are less compared with CFX@CS/PS-TPP. The sample loaded with the drug gives almost spherical-shaped particles (as shown in scanning electron microscopy (SEM) images) with satisfactory size dispersion.

3.3. In Vitro Drug Release Behavior. The in vitro release profiles of CFX are listed in Figure 6a. During the first 8 h, the % drug release was about 27, 33, and 47% for pH 7.4, 3.4, and 5.0, respectively. Such an initial burst of release was mainly due to the drug originally absorbed on the tight surface of the nanocomposite. After 8 h, the initial burst slightly decreased, and the cumulative drug release profiles maintained a sustained release. The CFX-loaded CS/PS-TPP nanocomposite exhibits a remarkable sustained-release property for all samples. However, the release rate of drug-loaded nanocomposite began to increase rapidly after 40 h, which might be due to the degradation of C.S.[39]

This work suggests that the administration route of the drug delivery system is oral. Because nanodrugs show higher oral bioavailability, they exhibit typical uptake mechanisms of absorptive endocytosis. Nanodrugs stay in the blood circulatory system for a prolonged period and enable the release of amalgamated drugs, as per the specified dose. Thus, they cause fewer plasma fluctuations with reduced adverse effects.

3.4. Fluorescence Quenching Mechanism. The fluorescence quenching of BHb-CFX, BHb-NCFX, and BHb-PS-CFX systems was analyzed using eq 3, and their corresponding Stern−Volmer plots of F_0/F vs [CFX], [NCFX], and [PS-CFX] are displayed in Figure 7a−d.

BHb possesses six tryptophan molecules (α-14 Trp, β-15 Trp, and β-37 Trp in each of the α and β chains). Intrinsic fluorescence of BHb primarily belongs to β-37 Trp located at $\alpha_1\beta_2$ interfaces as explained by Akram et al.[40] However, hemoglobin shows low fluorescence intensity in water as the efficient energy transfer from Trp to BHb significantly quenches the protein's fluorescence. The drug molecules (CFX) quenched the fluorescence intensity of Trp in the microenvironment system, accompanied by a red shift in the λ_{max} of about 8 nm (Figure 7a). It is clear from fluorescence spectra (Figure 7b) that the increase in the concentration of NCFX causes a decrease in the intensity of BHb without any shift. For CFX-PS1 and CFX-PS2 systems, the anticipated results indicate that the fluorescence intensity of BHb increased after the addition of

https://doi.org/10.1021/acsomega.3c04632
ACS Omega 2024, 9, 6339−6354

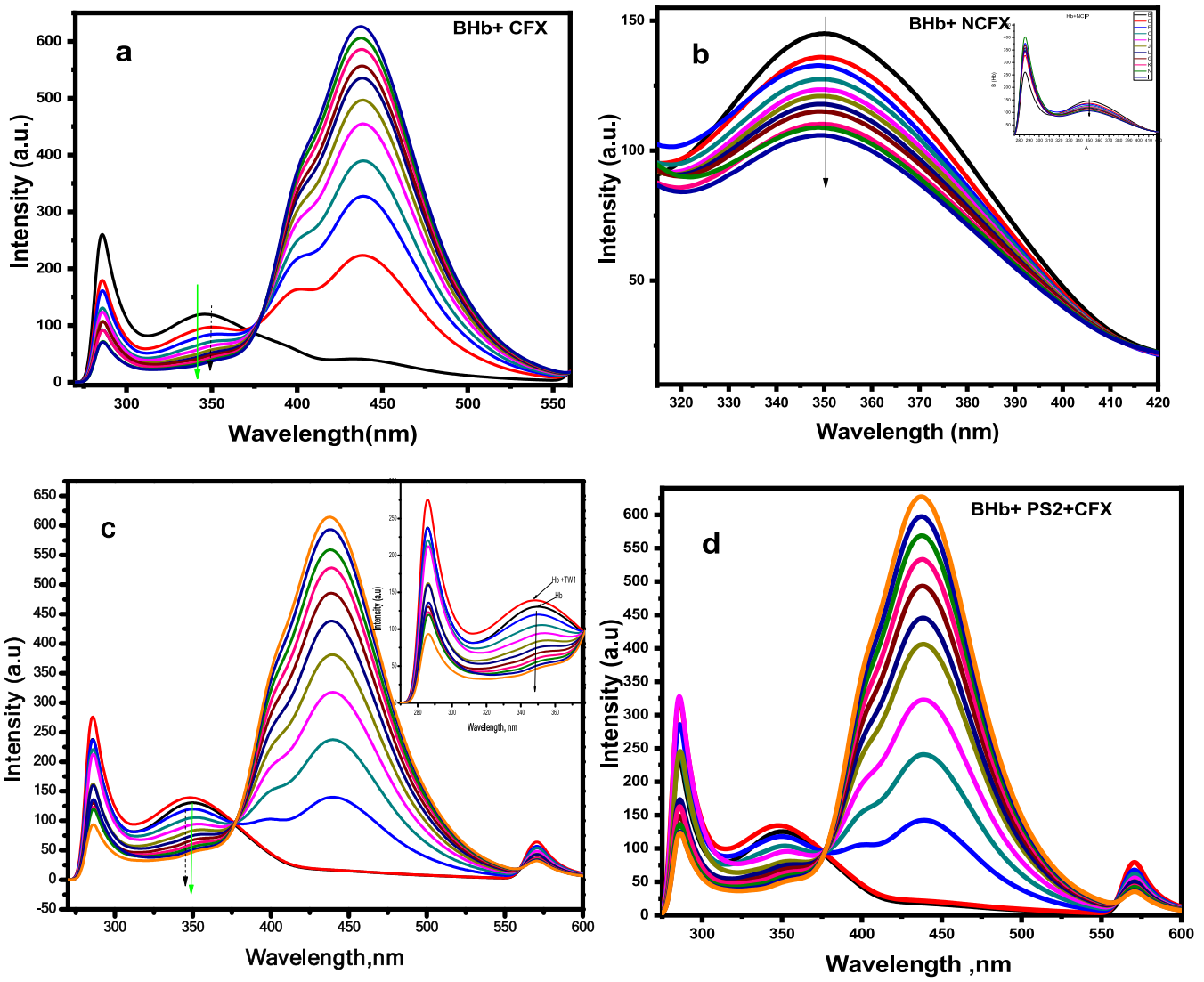

Figure 7. Emission spectra of BHb $C_{(BHb)}$ = 10 μM in the presence of various concentrations of (a) CFX (0.5−5) × 10^{-5} M and (b) NCFX (0.5−5) 10^{-5} M; effect the inclusion of (c) 1 μM PS-80 and (d) 2 μM PS-80 on the interaction of BHb with various concentrations of CFX $C_{(BHb)}$ = 10 μM; C_{CFX}; (0.5−4) μM.

polysorbate-80 (P.S.) (Figure 7c,d). In the presence of surfactant, hydrophobic interactions come into play that cause its hydrophobic chains to interact with the hydrophobic heme cavity of hemoglobin. Thus, increased distance between the Trp and heme reduces the quenching reaction between them, causing an enhancement in the quenching constants of the interaction CFX with BHb in the presence of "PS1 and PS2". The decrease in fluorescence intensity at $\Delta\lambda$ = 345 nm with blue shift (5 nm) revealed that the interaction of CFX with protein in the presence of polysorbate-80 resulted in an alteration microenvironment around tryptophan residue and moved it to a less hydrophobic environment.[41] On the other hand, at 10 higher concentrations of the quencher, the fluorescence intensity of BHb becomes almost constant. This is an outcome of the complete solubilization of heme in the micellar aggregates.

3.5. Binding and Quenching Constants. On the basis of pharmacokinetics, the binding affinity can be determined to know the bioavailability of drugs in the biological system. In general, K_A of more than 10,000 indicates that the binding is firm. The binding constant values of CFX, NCFX, CFX-PS2, and CFX-PS2 to BHb were 2.16 × 10^{-5}, 1.60 × 10^{-5}, 5.75 × 10^{-5}, and 9.90 × 10^{-5} mol L^{-1}, respectively, as listed in Table 2, indicating that there was a strong binding interaction of all systems with BHb. The drug in nano form NCFX has shown less binding affinity to BHb, which means that the absorption and distribution of the drug to various tissues would be higher due to

Table 2. Binding Parameters of the Interaction for Different Systems between BHb and Drugs λ_{ex} = 280 nm, pH 7.4

	T (K)	K_A (L^{-1}mol) × 10^{-5}	n	R^2	s.d.[a]
CFX-BHb	298	2.16	1.16	0.998	0.077
	304	1.09	1.09	0.999	0.016
	310	0.72	1.08	0.998	0.013
NCFX-BHb	298	1.60	1.3	0.990	0.200
	304	0.78	1.27	0.988	0.210
	310	0.50	1.28	0.996	0.120
CFX−BHb−PS_1	298	5.75	1.28	0.999	0.014
CFX−BHb−PS_2	298	9.90	1.36	0.995	0.036

[a]Standard deviation.

https://doi.org/10.1021/acsomega.3c04632
ACS Omega 2024, 9, 6339−6354

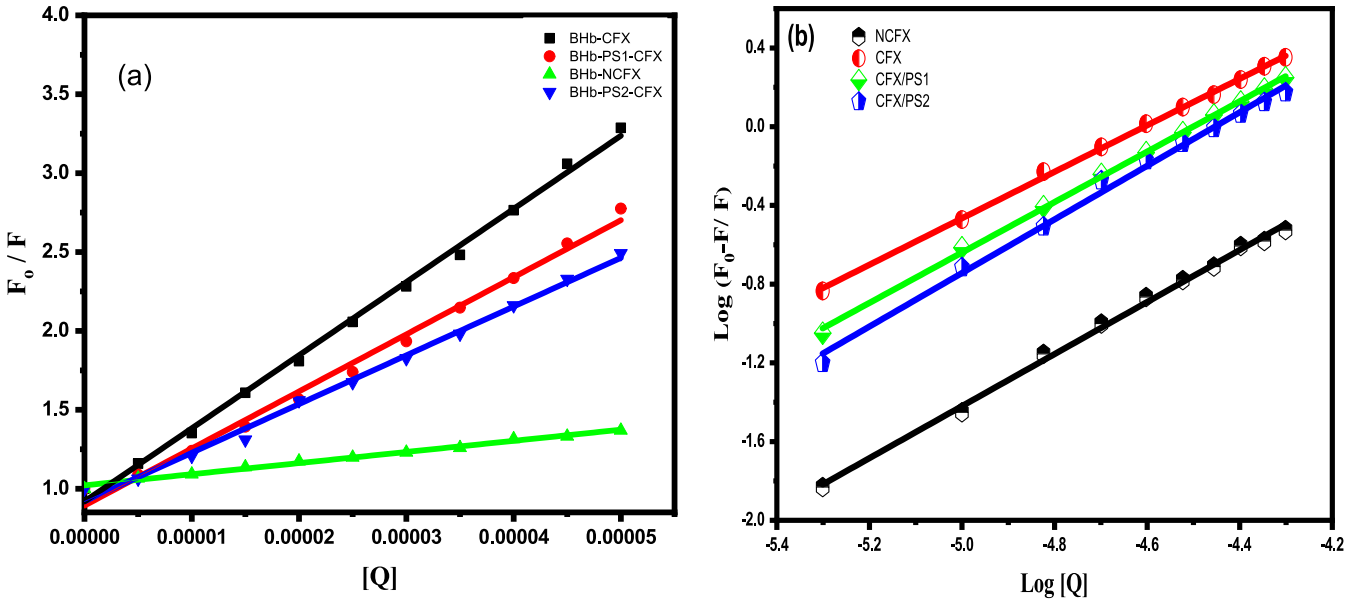

Figure 8. (a) Stern−Volmer plots describing BHb quenching of CFX, C_{BHb} = 10 μM; CFX (0.5−5) μM at 298 °K, pH 7.4, λ_{ex} = 280 nm. (b) Plots of $\log(F_0 - F)/F$ versus log[Q].

Table 3. Stern−Volmer Equation Constants and Bimolecular Quenching Rate Constants for the Interaction of CFX and NCFX with BHb at Various Temperatures, λ_{max} (280); pH (7.4)

	T (K)	K_{SV} (L^{-1} mol) × 10^{-4}	k_q (L mol^{-1} S^{1-}) × 10^{-12}	R^2	s.d.[a]
CFX-BHb	298	4.60	4.60	0.996	0.0260
	304	3.71	3.71	0.998	0.0116
	310	3.27	3.27	0.997	0.0142
NCFX-BHb	298	0.63	0.71	0.991	0.0056
	304	0.43	0.43	0.991	0.0053
	310	0.30	0.30	0.997	0.0030
CFX−BHb−PS_1	298	3.62	3.62	0.991	0.0320
CFX−BHb−PS_2	298	3.09	3.09	0.993	0.0230

[a]Standard deviation.

the stability of the NCFX-BHb complex being lower those of the CFX-BHb and CFX-PS-BHb complexes.[42]

The number of binding sites (n) can also be measured according to the fluorescence quenching experiments. The practical results indicated that BHb might have only one equivalent binding site for all cases (CFX, NCFX, CFX-PS2, and CFX-PS2), suggesting a complex formation between the drug and BHb in 1:1 mol L^{-1} concentration ratios.

As shown in Figure 8a,b, the plot exhibited an excellent linear relationship within the investigated concentrations of all systems. The value of Stern−Volmer quenching constants K_{SV} were obtained from the slope of the linear plot, and their values are listed in Table 3. In the presence of (PS1) and (PS2), the K_{SV} values were found to be smaller as compared to in its absence. This observation suggested that the Polysorbate-80 assists the release of CFX in a controlled manner because in the presence of ciprofloxacin, a fraction of CFX is bound to it, and weaker binding of CFX and Polysorbate-80 freely released more drug to the tissues as compared to the drug released from plasma.

3.6. Synchronous Fluorescence. Conformational changes that occurred in the structure of hemoglobin upon binding with CFX, NCFX, and CFX/PS were evaluated by using synchronous fluorescence. Synchronous fluorescence technique was used to provide the details about Tyr residues or Trp residues of BHb.[43] Since the interval ($\Delta\lambda$) values between the excitation (λ_{ex}) and emission (λ_{em}) wavelengths are adjusted at 15 or 60 nm, all of the changes occurring around the amino acids Tyr and Trp residues can be observed from the emission shift of synchronous fluorescence spectra.[19] BHb contains three Trp residues and three Tyr residues in each α β dimer. The Trp and Tyr residues are symmetric, with the BHb cavity as the symmetry center. The synchronous spectra of BHb when the $\Delta\lambda$ was 60 and 15 nm, in the absence and presence of increasing drug to BHb (from 0.5 to 4.0 × 10^{-5} M), were shown in (Figure 9a−f). The fluorescence intensity of BHb (Tyr and Trp) residues gradually decreases in all cases on the addition of CFX (Figure 9a,b), NCFX (Figure 9c,d), and in the system CFX-PS (Figure 9e,f). These results in Figure 9a−f revealed that the fluorescence of tyrosine and tryptophan residues in BHb was quenched by CFX, NCFX, and CFX/PS, indicating that the molecules could enter the three-dimensional structure of BHb, not only could directly destroy the fluorescence of tryptophan residues but also could block the energy transfer between tyrosine and tryptophan. At the same time, with the increase of CFX concentration, a slight red shift (10 nm) was found at the maximum (λ_{em}) of Trp residues, as shown in Figure 9b, while in the case of the CFX-PS system (Figure 9f), a slight red shift (5 nm) was lower compared to the CFX-BHb system due to the presence of surfactant at the maximum λ_{em} of Trp residues. In the NCFX system, the maximum λ_{em} Trp residue was not changed. The maximum λ_{em}

https://doi.org/10.1021/acsomega.3c04632
ACS Omega 2024, 9, 6339−6354

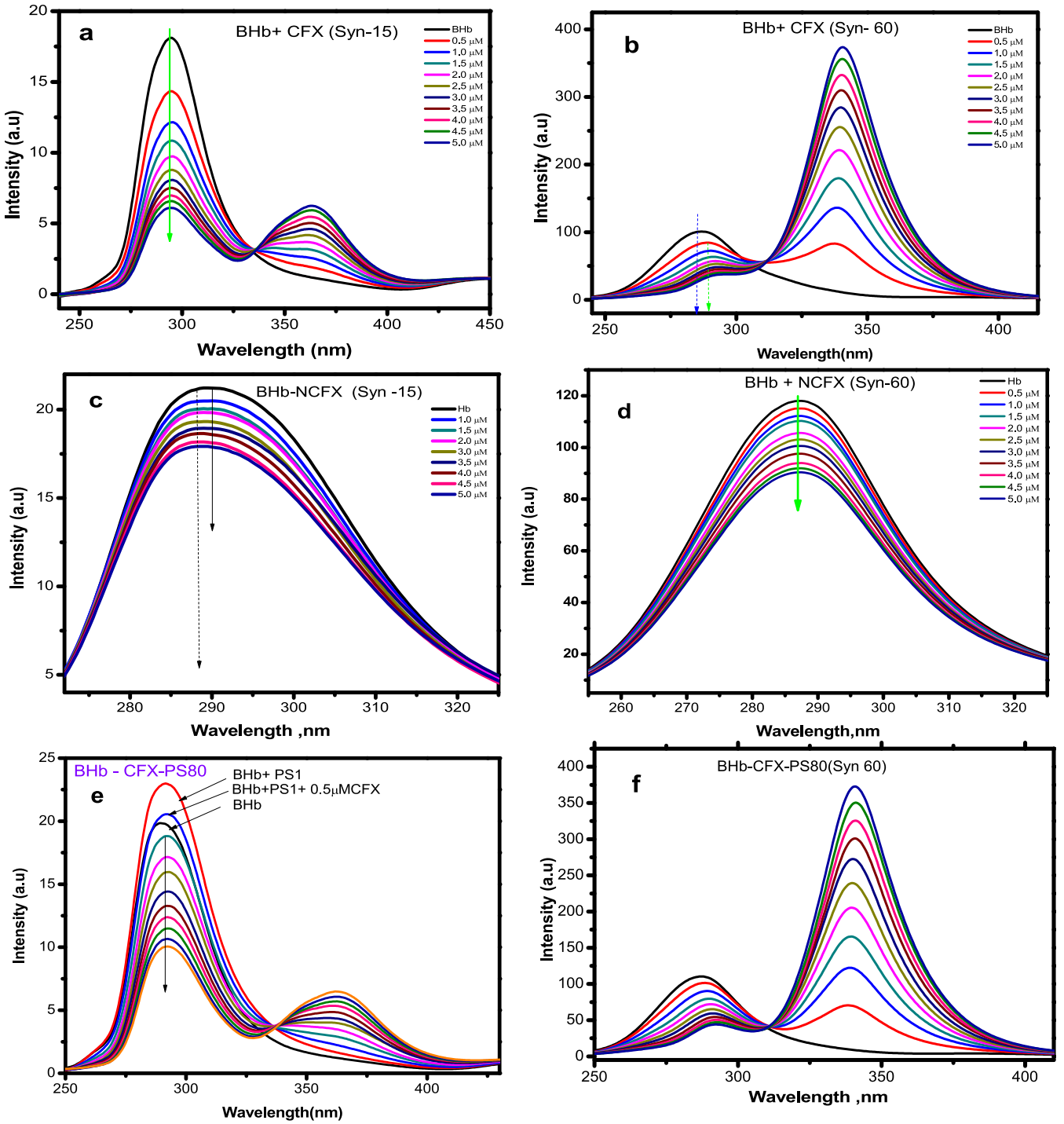

Figure 9. Synchronous fluorescence spectra of (a) BHb-CFX at $\Delta\lambda$ = 15 nm, (b) BHb-CFX at $\Delta\lambda$ = 60 nm, (c) BHb-NCFX at $\Delta\lambda$ = 15 nm, (d) BHb-NCFX at $\Delta\lambda$ = 60 nm, (e) BHb-PS-CFX at $\Delta\lambda$ = 15 nm, and (f) BHb-PS-CFX at $\Delta\lambda$ = 60 nm.

of Tyr residues almost did not change in all cases, indicating that the slight decrease in the hydrophobicity surrounding Tyr residues but almost no change in the hydrophobicity surrounding Tyr residues except in NCFX case might be due to the size of molecules; these results revealed that the conformation of BHb was changed.

3.7. Thermodynamic Studies. Thermodynamic studies and Van't Hoff equation were explored by two methods, and plots of F_0/F against [Q] and also $\log\left[\frac{F_0 - F}{F}\right]$ versus log[Q] for CFX and NCFX as quenchers with BHb at different temperatures (298−310 K) are shown in Figure 10a−d, respectively, indicating the excellent linearity relationship and the corresponding values of K_{SV} were calculated from the slope of curves. The quenching of fluorescence is known to occur by two procedures, namely, dynamic (collisional) quenching and/or static quenching, since the formation of a complex between the quencher (drug) and the fluorophore.[44]

The experimental results indicated that the K_{SV} values were increased with increasing temperature. The k_q values were found to be greater than the maximum scattering collision quenching rate constant (2.0×10^{10} L mol^{-1} S^{1-}) as listed in Table 3. The

https://doi.org/10.1021/acsomega.3c04632
ACS Omega 2024, 9, 6339−6354

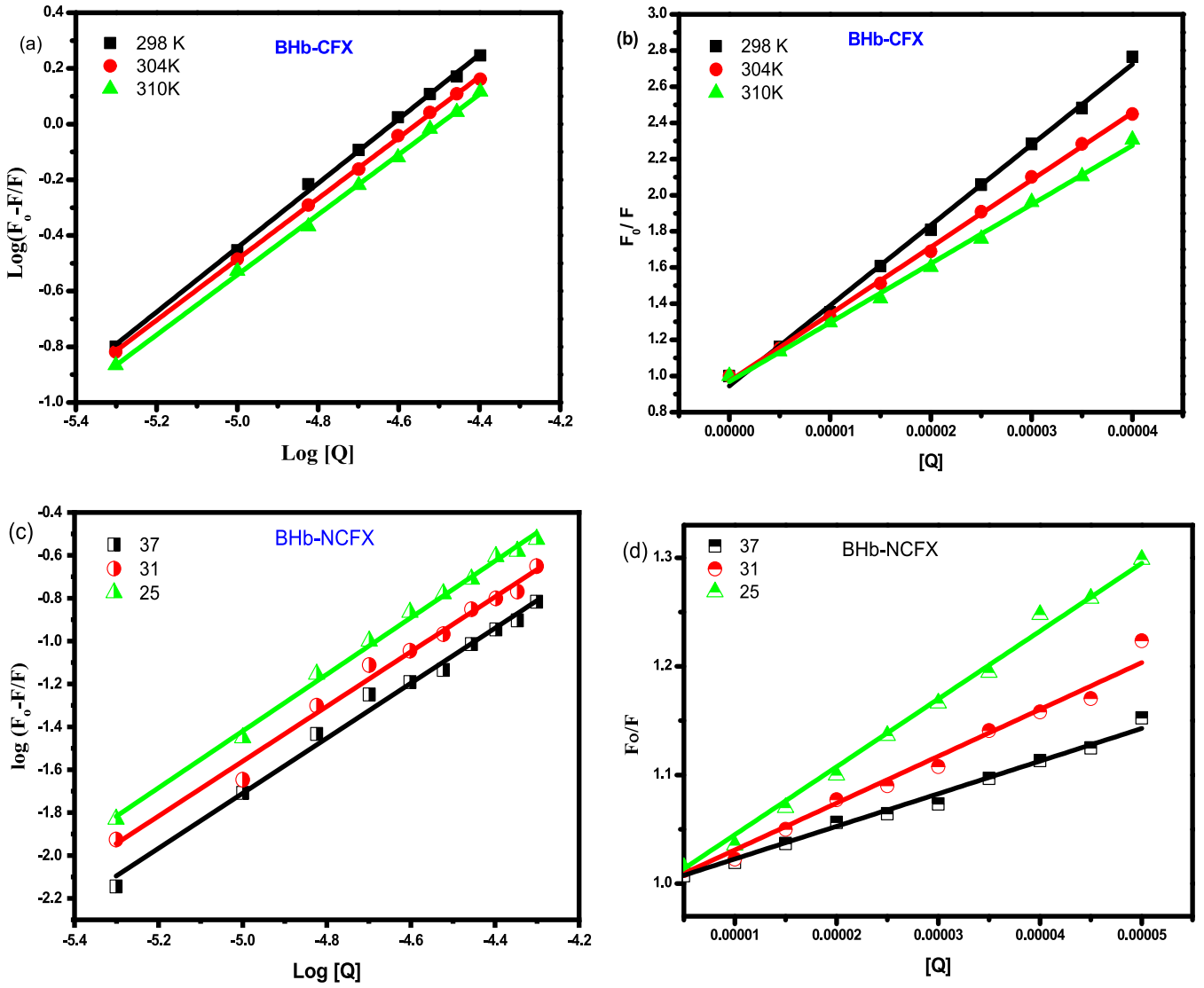

Figure 10. (a, c) Modified Stern–Volmer plots with $\log(F_0 - F)/F$ v/s $\log[Q]$, hence C_{BHb} = 10 μM; C_{CFX} and C_{NCFX} (0.5–5) μM at various temperatures, pH = 7.4. (b, d) Stern–Volmer plots for describing BHb quenching of CFX and NCFX, hence C_{BHb} = 10 μM, C_{CFX} and C_{NFCX} (0.5–5) μM at various temperatures (pH = 7.4).

Van't Hoff plot for the temperature dependence of K_{SV} and K_A values was calculated from fluorescence quenching of BHb with CFX and NCFX as listed in Table 4, and their plots are shown in Figure S1, indicating that the fluorescence quenching mechanisms were a static process, which suggested that the BHb–drug complex is probably formed during the interaction.

As reported by Ross and Subramanian, the signs and magnitudes of the thermodynamic parameters (ΔH and ΔS) are associated with various individual kinds of interaction that may occur in the protein association process.[45] That is, if $\Delta H > 0$ and $\Delta S > 0$, the main force is hydrophobic interaction. If $\Delta H < 0$ and $\Delta S < 0$, van der Waals and hydrogen bonding interactions play significant roles in the reaction, while the negative ΔH^0 and positive ΔS^0 values are considered as evidence for electrostatic interactions between ionic species in aqueous solution. This study listed thermodynamic parameters in Table 4; the negative values of ΔG indicated the spontaneity of the binding interactions between CFX and NCFX with BHb. However, the negative signs of ΔH and ΔS suggested that the hydrogen bonding and van der Waals forces interactions play a significant role in the reaction. The structural changes of BHb by adding various systems CFX, CFX-PS, and NCFX were studied.

Table 4. Thermodynamic Parameters Interactions of CFX and NCFX with BHb

	T (K)	ΔG (kJ)	ΔH (kJ mol^{-1})	ΔS (J/mol K)	R^2	s.d.
CFX-BHb	298	−30.51				
	304	−29.30	−72.17	−140.8	0.99	0.17
	310	−28.46				
NCFX-BHb	298	−29.52				
	304	−28.60	−74.7	−151.6	0.98	0.57
	310	−25.70				

3.8. FRET Analysis. The overlap of the absorbance spectra of CFX and NCFX with the emission spectrum of HBb (λ_{ex} = 280 nm) is presented in Figure 11a,b. In a proteinous environment, the proximity of the ligand molecule to the tryptophan moiety is often determined through a FRET study.

The J, E, R_0, and r parameters were calculated using eqs 9, 10, and 11 and listed in Table 5. An essential criterion for the

https://doi.org/10.1021/acsomega.3c04632
ACS Omega 2024, 9, 6339–6354

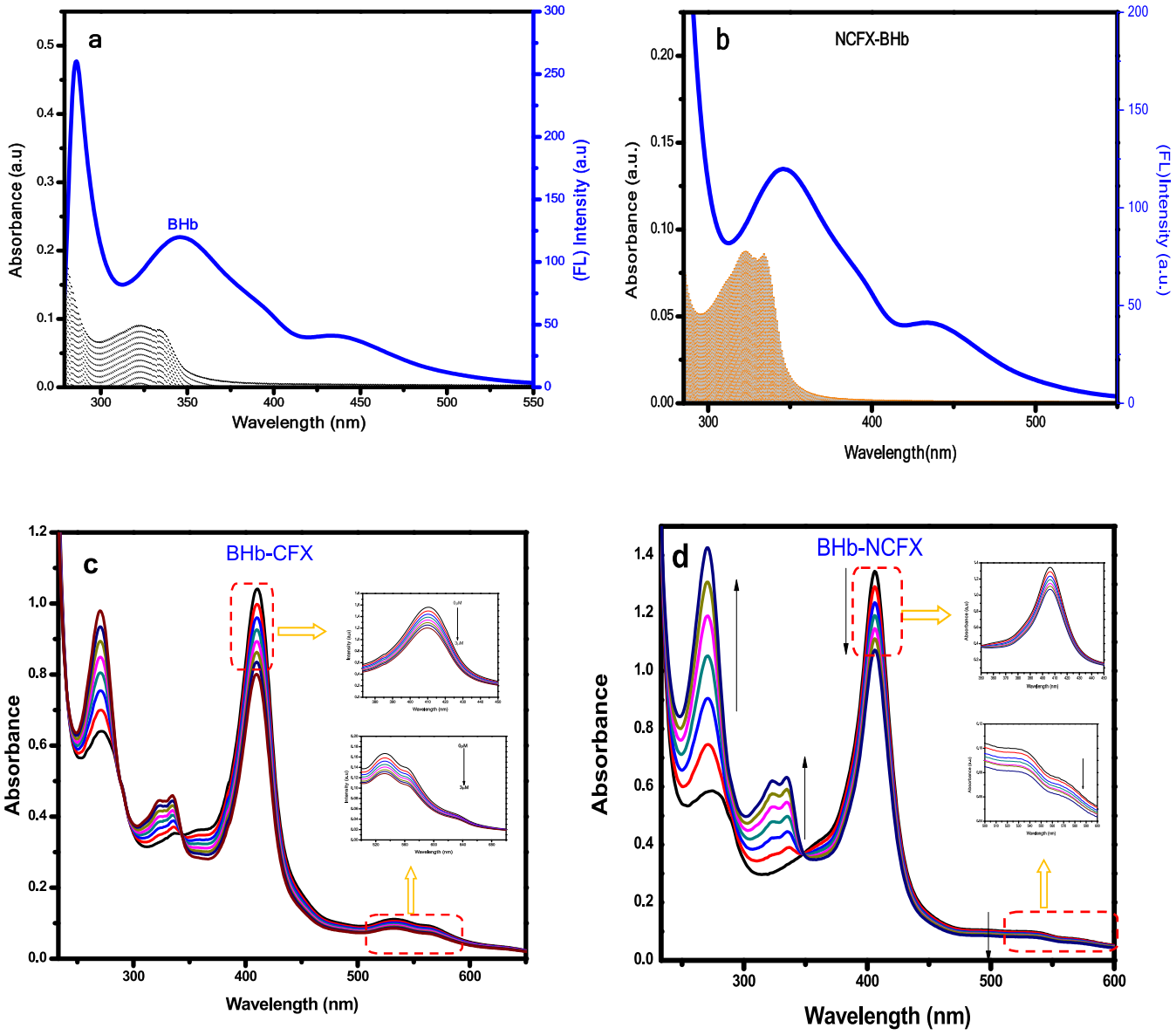

Figure 11. (a, b) Overlapping of the absorbance spectra of CFX and NCFX with the emission spectrum of HBb (λ_{ex} = 280 nm). (c, d) UV−vis spectra of BHb in the presence of (a) CFX; $C_{(BHb)}$ = 10 μM, $C_{(CFX)}$ = (0.5−5) μM (b) NCFX- BHb $C_{(BHb)}$ = 10 μM and $C_{(CFX)}$ = (0.5−5) μM.

Table 5. FRET Parameters Obtained from CFX and NCFX Binding to BHb

system	J (cm^3 L mol^{-1})	E (%)	R_0 (nm)	r (nm)
BHb-CFX	1.99×10^{-14}	0.199	2.45	1.71
BHb-NCFX	3.93×10^{-14}	0.210	2.73	1.73

binding distance "r" between donor and acceptor must be $r < 7$ nm and $0.5R_0 < r < 1.5R_0$, and the values of distance "r" obtained were found to be 1.71 and 1.73 nm for CFX and NCFX, respectively. The results indicated that the energy transferred from BHb to CFX and NCFX occurred with a high possibility.[24] Further, the energy transfer phenomena also suggested that CFX and NCFX could strongly quench the intrinsic fluorescence of BHb by a static quenching mechanism.[25]

3.9. UV−Vis Studies. The UV−vis absorption spectra of BHb in the presence and absence of CFX and NCFX drugs are shown in Figure 11c,d. The spectra show an electronic band (globin band) at around 280 nm due to the phenyl group of Trp and Tyr residues. The value of λ_{max} at about 406 nm, Soret peak due to heme group, is observed. Furthermore, the ε-band at 349 nm and oxy-band or Q-band at around 540 and 576 nm are also observed.[46] The absorption intensity of BHb at around 406 nm was decreased with increasing CFX and NCFX concentrations. These results suggested that compound formation rather than dynamic collision initiated the probable quenching mechanism of the Ciprofloxacin−HCl drug with -BHb binding reaction. The blue shift of CFX-BHb and NCFX-BHb complexes (280 nm) revealed that the conformation and/or microenvironment of BHb were altered in the presence of CFX.

3.10. CD Analysis. Circular dichroism (CD) analyses were carried out in the presence of different CFX, NCFX, and CFX/PS concentrations to ascertain the secondary structure changes of BHb molecules quantitatively (Figure 12a−c). There were two main negative bands in the far-UV region at 208 and 222 nm, which is characteristic of the α-helical structure of BHb. The CD results quantitatively demonstrate a perturbation of the secondary structure of BHb following interaction with CFX as

https://doi.org/10.1021/acsomega.3c04632
ACS Omega 2024, 9, 6339−6354

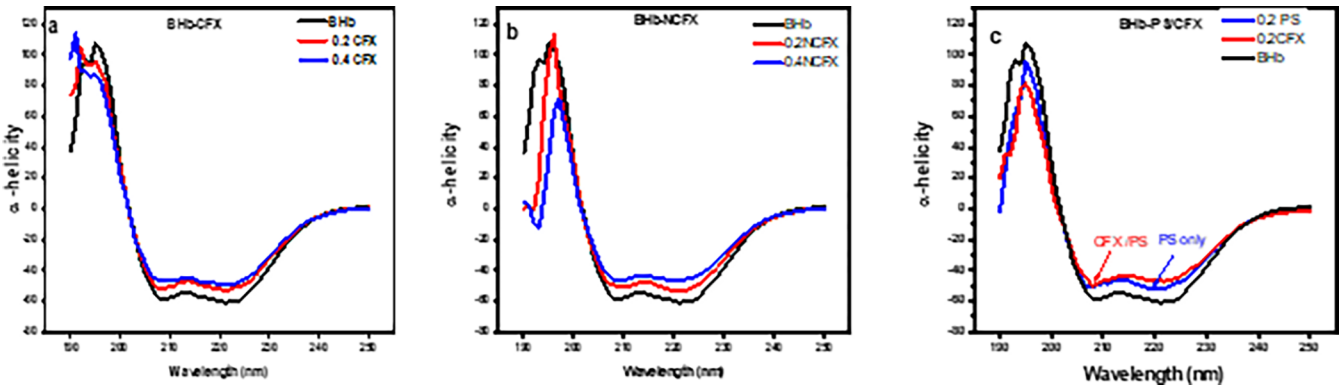

Figure 12. CD spectra of (A) HBA (10 μM) in pH 7.40 phosphate buffer at different concentrations of (a) CFX, (b) NCFX, and (c) CFX/PS at 298 K.

evidenced by a loss in the α-helicity content (from ~43.3 (±2) % in native BHb (in the absence of CFX) to ~37 (±2) % in the presence of 50 μM CFX, Figure 12a). For NCFX (Figure 12b), the loss in α-helicity content was 34 (±2) % in the presence of 50 μM NCFX. The content of α-helix in BHb was calculated using (eq 12) and the corresponding values are summarized in Table 6.

Table 6. Secondary Structural Analysis of the Varied Molar Ratio of CFX and NCFX Drugs with BSA (10 μM) from CD Data (pH 7.4, T = 298 K)

system	CFX	NCFX	mole ratio [BHb: drug]
α-helix (%)	43.449	43.449	0 μM
	38.943	38.430	1:0.2
	37.254	34.437	1:0.4

3.11. Three-Dimensional (3D) Analysis. The contour map and 3D emission spectra of BHb in the absence and presence of CFX, NCFX, and CFX-PS are shown in Figure 13a–d. The corresponding characteristic parameters are given in Table 7. As shown in Figure 13a, the 3D emission spectra of BHb show three peaks: peaks 1, *a*, and *b*. Peak 1 is the first-order Rayleigh scattering peak (λ_{em} & λ_{ex}). Peak *a* (λ_{ex} = 280 nm) is mainly attributed to the characteristic intrinsic emission spectral behavior of Trp and Tyr residues. It must be noted that the absorption spectrum of BHb (Figure 13a) shows an absorption maximum at 440 nm due to pi–pi* transition of aromatic amino acid residues, viz., Trp, Tyr, and phenylalanine (Phe) that occur in the binding cavity of BHb. Peak *b* (λ_{ex} = 330 nm) in BHb is mainly caused by the characteristic transition of *n*–pi* of the polypeptide backbone. The 3D emission for the BHb-CFX system (Figure 13b) shows a new peak belonging to CFX, revealing that the polarity of the microenvironment around Tyr and Trp residues and the conformation of BHb were changed.

3.12. Molecular Docking. It can be seen from Figure 14A that CFX preferentially binds to the hydrophobic cavity formed by α1, α2, and β2 subunits of BHb. Moreover, Tyr-144 B can be seen interacting with the two aromatic rings of CFX through π–π interaction. It should be noted that it is the Trp and Tyr residues that are responsible for the absorbance peak of the globin band of BHb and the direct interaction (π–π) of Tyr-144 (Figure 14A) with the two aromatic rings that appraise the origin of the absorbance enhancement in the globin band. The BHb-CFX system has two hydrogen bonds between CFX and BHb amino acid residues. Hydrogen bonds were established between oxygen of ketone and carboxyl groups of CFX with Asn107 and Gln130 amino acid residues, while van der Waals forces were between CFX and amino acids residues of Pro37, Lys131, Leu104, and Val133. Moreover, the hydrophobic interactions among CFX and Lys103 (mixed π–alkyl hydrophobic forces), Phe36 (π–π hydrophobic forces), and Ala134 (π–σ) amino acid residues of BHb were observed. The binding energy of CFX-BHb was found to be −7.1 kcal mol^{-1} (−29.7 kJ mol^{-1}) (Table S1) which is close to the experimental results of ΔG° binding (−30.5 kJ mol^{-1}). Furthermore, the docking findings provide an excellent structural basis to explain the efficient fluorescence quenching of the fluorophore, which was found to be about 76%.

4. CHARACTERIZATION

All biophysical investigations were conducted with reproducibility and a standard deviation approach for obtained results. An F-2700 FL spectrophotometer with scan rate (1500 nm/min), EX slit 5 nm was used for synchronous and fluorescence studies.[47] UV–Vis measurements were recorded by a PerkinElmer U.V Win Lab 6.0.4.0738/1.61.00 Lambda 800 spectrometer. FT-IR analysis was performed in a moisture-free atmosphere using PerkinElmer electronic. TGA–DTA analyses of the samples have been studied by a PerkinElmer instrument, with temperature ranging from room temperature to 800 °C in a nitrogen chamber at a heating rate of 5 °C/min. XRD patterns were performed using a Lab X, SHIMADZU XRD-6100 instrument (Japan). The instrument was equipped with a rotation anode operating using copper-filtered Kα radiation at 40 kV[48,49] and 30 mA. The size of nanoparticles was measured by using dynamic light scattering (DLS), a digital correlation system (Malvern2008-V 2.3 (Zetasizer)-Hellma, GmbH, and U.K.). The samples' morphology was recorded using a scanning electron microscope (SEM) JEOL (Japan) JSM-6510 with an accelerating voltage of 15 kV.

5. CONCLUSIONS

The ciprofloxacin-HCl drug was successfully encapsulated on the surface of the CS/PS-TPP nanocomposite, and it was further used for drug delivery application. A biophysical investigation was conducted to understand the interaction of CFX and NCFX with bovine hemoglobin. The effects of polysorbate-80 inclusion on release drug and CFX binding with BHb were studied. The results suggested that the binding of CFX was reduced with BHb when delivered from micellar media, indicating that the presence of surfactant improved the loading and release of the CFX drug. The binding constants of CFX, NCFX, and CFX/PS with BHb were found to have values of 2.16 × 10^5, 1.6 × 10^5, 5.75 × 10^5,

https://doi.org/10.1021/acsomega.3c04632
ACS Omega 2024, 9, 6339–6354

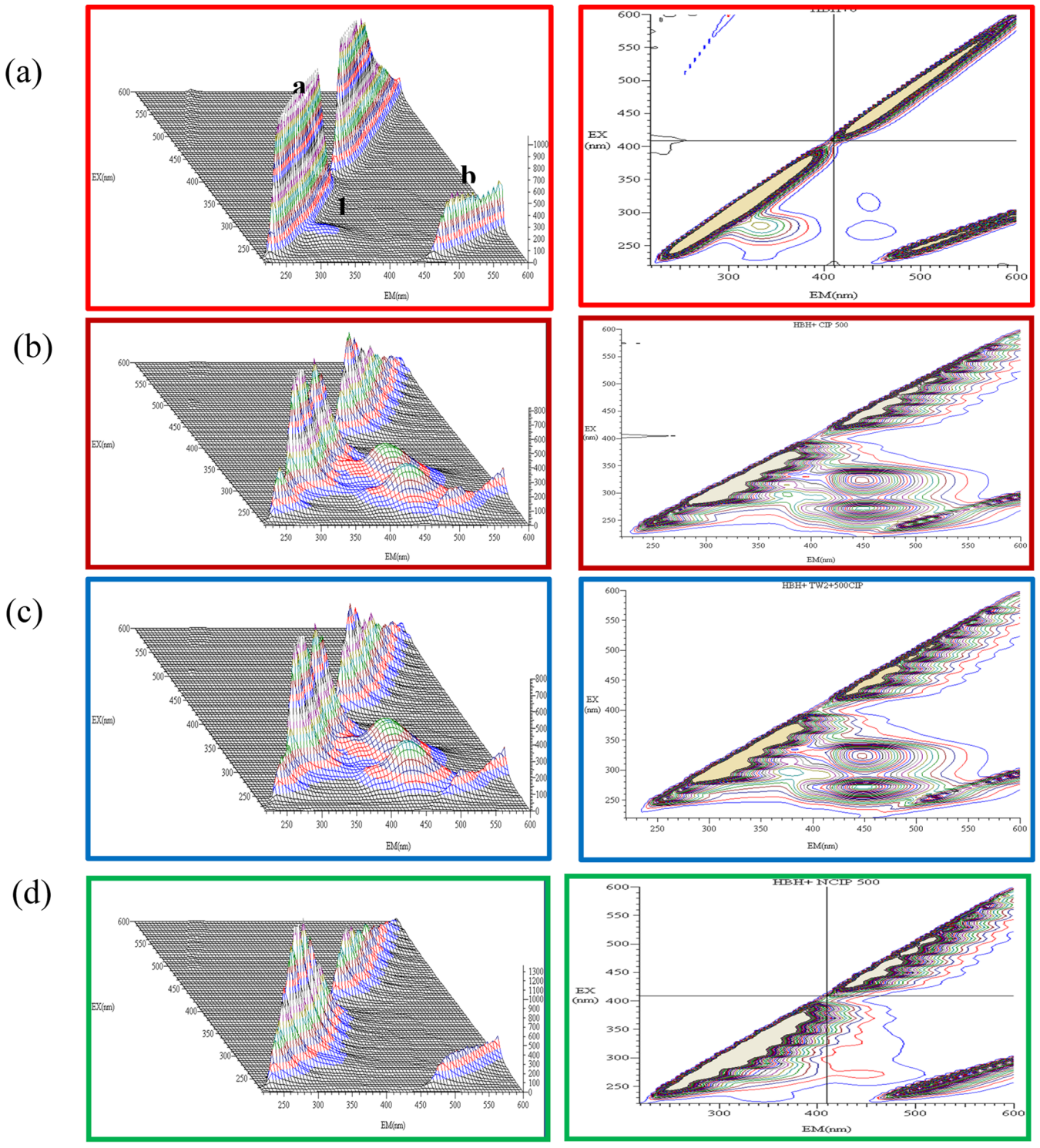

Figure 13. Three-dimensional fluorescence diagrams of (a) BHb only, (b) CFX-BHb system, (c) CFX/PS-BHb system, and (d) NCFX-BHb system.

Table 7. 3D Fluorescence Spectral Characteristic Parameters of BHb and CFX-BHb Systems

system	CFX (μM)	peak (nm)	intensity (a.u.)
BHb	0	270/440	15.0
BHb	0	280/335	75.0
BHb−CFX	2.5	270/450	267.3
BHb−CFX	2.5	325/450	245.9
BHb−NCFX	2.5	270/450	23.33

and 9.90×10^5 mol L^{-1}, respectively. The results revealed that the mechanism of fluorescence quenching of BHb by CFX and NCFX was found to be statically together with a spontaneous binding process and enthalpically driven, involving both hydrogen bonding and van der Waals forces. Synchronous fluorescence spectra showed an alteration in the microenvironment around tryptophan and tyrosine residues. The binding of BHb and CFX or NCFX induced the microenvironment around amino acid residues in BHb. The 3D emission spectra of the BHb − CFX system showing new peaks belonging to CFX

https://doi.org/10.1021/acsomega.3c04632
ACS Omega 2024, 9, 6339−6354

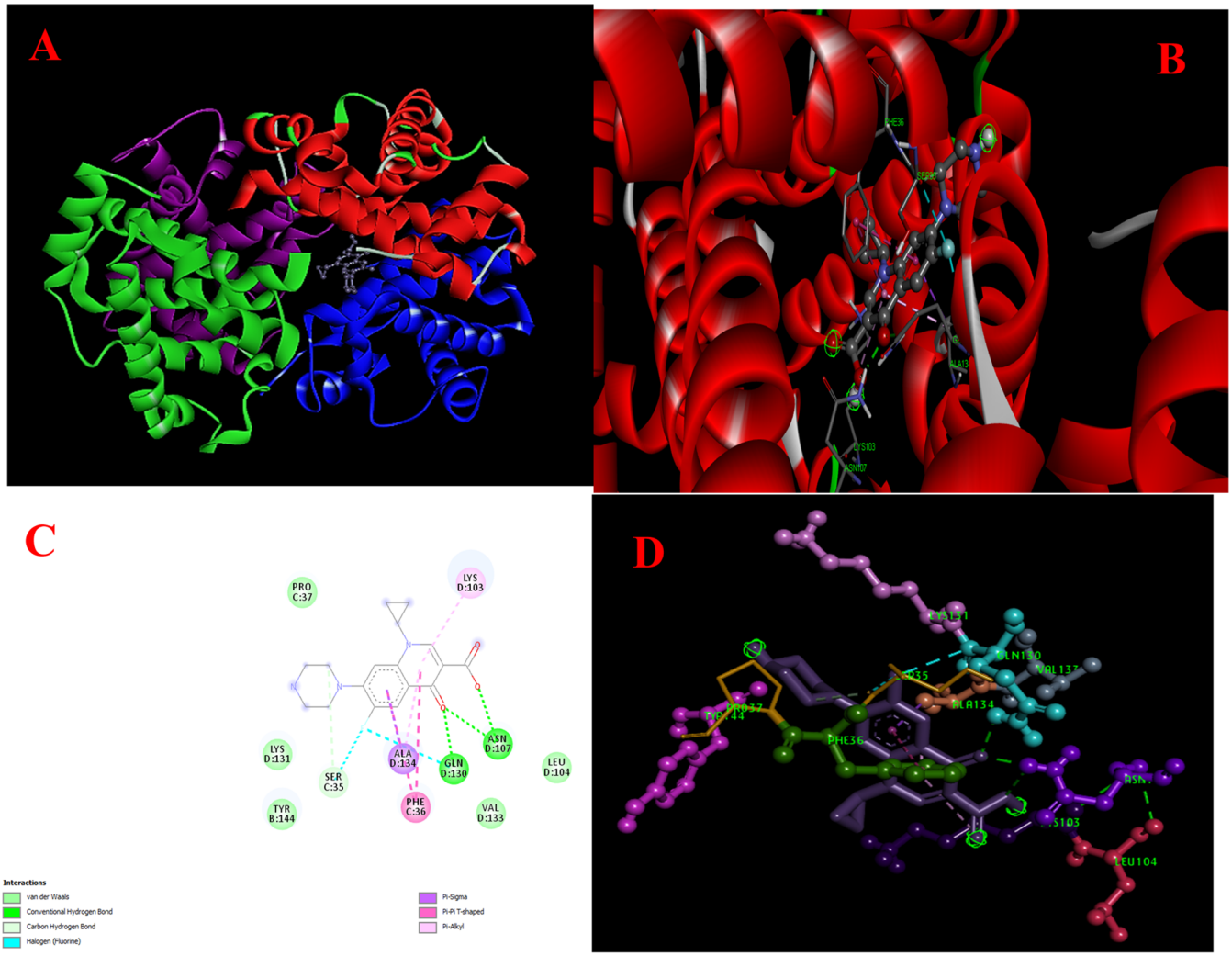

Figure 14. (A–D) Lowest binding energy docked conformation for CFX on BHb (A); amino acid residues surrounding CFX (B) binding pocket for CFX-BHb system; (C) 2D binding for CFX-BHb system; and (D) 3D binding sites for CFX on BHb.

revealed that the polarity of the microenvironment around Tyr and Trp residues and the conformation of BSA were changed.

■ ASSOCIATED CONTENT

Supporting Information

The Supporting Information is available free of charge at https://pubs.acs.org/doi/10.1021/acsomega.3c04632.

Van't Hoff plot of $\ln K$ vs $1/T$ for elucidation of the thermodynamic parameters for the CFX and NCFX – protein (BHb) interaction process (Figure S1) and docking summary of BHb with CFX (Table S1) (PDF)

■ AUTHOR INFORMATION

Corresponding Authors

Yahiya Kadaf Manea – *Department of Chemistry, University of Aden, 6312 Aden, Yemen;* orcid.org/0009-0001-9853-2544; Email: Yahiaka.chem.edu@univ-aden.net

Mashallah Rezakazemi – *Faculty of Chemical and Materials Engineering, Shahrood University of Technology, 3619995161 Shahrood, Iran;* orcid.org/0000-0002-9980-6682; Email: mashalah.rezakazemi@gmail.com

Author

Mohsen T. A. Qashqoosh – *Department of Chemistry, University of Aden, 6312 Aden, Yemen; Department of Chemistry, Aligarh Muslim University, Aligarh 202002, India*

Complete contact information is available at: https://pubs.acs.org/10.1021/acsomega.3c04632

Notes

The authors declare no competing financial interest.

■ ACKNOWLEDGMENTS

The authors thank the Chairman, Department of Chemistry, Aligarh Muslim University, Aligarh, India, for providing research facilities. Y.K.M. is thankful to the University of Aden, Yemen, for providing financial assistance.

■ REFERENCES

(1) Hanna, D. H.; Saad, G. R. Encapsulation of Ciprofloxacin within Modified Xanthan Gum- Chitosan Based Hydrogel for Drug Delivery. *Bioorg. Chem.* **2019**, *84*, 115–124.

(2) Nitta, S. K.; Numata, K. Biopolymer-Based Nanoparticles for Drug/Gene Delivery and Tissue Engineering. *Int. J. Mol. Sci.* **2013**, *14* (1), 1629–1654.

(3) Wu, D.; Zhai, Y.; Yan, J.; Xu, K.; Wang, Q.; Li, Y.; Li, H. Binding Mechanism of Tauroursodeoxycholic Acid to Human Serum Albumin: Insights from NMR Relaxation and Docking Simulations. *RSC Adv.* **2015**, *5* (15), 11036−11042.
(4) Buhus, G.; Popa, M.; Desbrieres, J. Hydrogels Based on Carboxymethylcellulose and Gelatin for Inclusion and Release of Chloramphenicol. *J. Bioact. Compat. Polym.* **2009**, *24* (6), 525−545.
(5) Ali, M. A.; Kaneko, T. Syntheses of Aromatic/Heterocyclic Derived Bioplastics with High Thermal/Mechanical Performance. *Ind. Eng. Chem. Res.* **2019**, *58*, 15958−15974.
(6) Singh, A. K.; Achazi, K.; Schade, B.; Haag, R.; Sharma, S. K. Synthesis of Non-Ionic Bolaamphiphiles and Study of Their Self-Assembly and Transport Behaviour for Drug Delivery Applications. *RSC Adv.* **2018**, *8*, 31777−31782.
(7) Yin, B.-T.; Yan, C.-Y.; Peng, X.-M.; Zhang, S.-L.; Rasheed, S.; Geng, R.-X.; Zhou, C.-H. Synthesis and Biological Evaluation of α-Triazolyl Chalcones as a New Type of Potential Antimicrobial Agents and Their Interaction with Calf Thymus DNA and Human Serum Albumin. *Eur. J. Med. Chem.* **2014**, *71*, 148−159.
(8) Hazra, S.; Hossain, M.; Suresh Kumar, G. Binding of Isoquinoline Alkaloids Berberine, Palmatine and Coralyne to Hemoglobin: Structural and Thermodynamic Characterization Studies. *Mol. BioSyst.* **2013**, *9* (1), 143−153.
(9) Ansari, S. S.; Yousuf, I.; Arjmand, F.; Siddiqi, M. K.; Naqvi, S. Exploring the Intermolecular Interactions and Contrasting Binding of Flufenamic Acid with Hemoglobin and Lysozyme: A Biophysical and Docking Insight. *Int. J. Biol. Macromol.* **2018**, *116*, 1105−1118.
(10) Manea, Y. K.; Khan, A. M. T.; Qashqoosh, M. T. A.; Wani, A. A.; Shahadat, M. Ciprofloxacin-Supported Chitosan/Polyphosphate Nanocomposite to Bind Bovine Serum Albumin: Its Application in Drug Delivery. *J. Mol. Liq.* **2019**, *292*, No. 111337.
(11) Makarska-Bialokoz, M. Interactions of Hemin with Bovine Serum Albumin and Human Hemoglobin: A Fluorescence Quenching Study. *Spectrochim. Acta, Part A* **2018**, *193*, 23−32.
(12) Deechongkit, S.; Wen, J.; Narhi, L. O.; Jiang, Y.; Park, S. S.; Kim, J.; Kerwin, B. A. Physical and Biophysical Effects of Polysorbate 20 and 80 on Darbepoetin Alfa. *J. Pharm. Sci.* **2009**, *98*, 3200−3217, DOI: 10.1002/jps.21740.
(13) Yan, X.; Liu, B.; Chong, B.; Cao, S. Interaction of Cefpiramide Sodium with Bovine Hemoglobin and Effect of the Coexistent Metal Ion on the Protein-Drug Association. *J. Lumin.* **2013**, *142*, 155−162.
(14) Das, S.; Bora, N.; Rohman, M. A.; Sharma, R.; Jha, A. N.; Roy, A. S. Molecular Recognition of Bio-Active Flavonoids Quercetin and Rutin by Bovine Hemoglobin: An Overview of the Binding Mechanism, Thermodynamics and Structural Aspects through Multi-Spectroscopic and Molecular Dynamics Simulation Studies. *Phys. Chem. Chem. Phys.* **2018**, *20* (33), 21668−21684.
(15) Liu, B.-S.; Yan, X.-N.; Cao, S.-N.; Chong, B.-H.; Yang, C.; Lü, Y.-K. Interaction of Salicylic Acid with Bovine Hemoglobin and Effect of the Coexistent Metal Ion on the Reaction. *Spectrosc. Lett.* **2013**, *46* (3), 165−174.
(16) Wang, Y.-Q.; Zhang, H.-M.; Zhou, Q.-H. Studies on the Interaction of Caffeine with Bovine Hemoglobin. *Eur. J. Med. Chem.* **2009**, *44* (5), 2100−2105.
(17) Xiao, M.; Yuan, X.; Xie, W.; Ge, X.; Zhou, Y.; Zhou, L.; Zhou, J.; Shen, J. Comparison of 9-Hydroxy-Artemisinin with Artemisinin: Interaction with Bovine Hemoglobin. *J. Lumin.* **2015**, *160*, 188−194.
(18) Chakraborti, A. S. Interaction of Porphyrins with Heme Proteins − a Brief Review. *Mol. Cell. Biochem.* **2003**, *253* (1/2), 49−54.
(19) Dasmandal, S.; Kundu, A.; Rudra, S.; Mahapatra, A. Binding Interaction of an Anionic Amino Acid Surfactant with Bovine Serum Albumin: Physicochemical and Spectroscopic Investigations Combined with Molecular Docking Study. *RSC Adv.* **2015**, *5* (96), 79107−79118.
(20) Otzen, D. Protein−Surfactant Interactions: A Tale of Many States. *Biochim. Biophys. Acta, Proteins Proteomics* **2011**, *1814* (5), 562−591.
(21) Banu, A.; Khan, R. H.; Qashqoosh, M. T. A.; Manea, Y. K.; Furkan, M.; Naqvi, S. Multispectroscopic and Computational Studies of Interaction of Bovine Serum Albumin, Human Serum Albumin and Bovine Hemoglobin with Bisacodyl. *J. Mol. Struct.* **2022**, *1249*, No. 131550.
(22) Manea, Y. K.; Banu, A.; Qashqoosh, M. T. A.; Khan, A. M.; Alahdal, F. M. A.; Wani, A. A.; Salem, M. A. S.; Naqvi, S. Interaction of AMOT@CS NPs and AMOT Drug with Bovine Serum Albumin: Insights from Spectroscopic and Molecular Docking Techniques. *Chem. Phys.* **2021**, *546*, No. 111139.
(23) Qashqoosh, M. T. A.; Alahdal, F. A. M.; Manea, Y. K.; Zakariya, S. M.; Naqvi, S. Synthesis, Characterization and Spectroscopic Studies of Surfactant Loaded Antiulcer Drug into Chitosan Nanoparticles for Interaction with Bovine Serum Albumin. *Chem. Phys.* **2019**, *527*, No. 110462.
(24) Sharma, G.; Naushad, M.; Thakur, B.; Kumar, A.; Negi, P.; Saini, R.; Chahal, A.; Kumar, A.; Stadler, F. J.; Aqil, U. Sodium Dodecyl Sulphate-Supported Nanocomposite as Drug Carrier System for Controlled Delivery of Ondansetron. *Int. J. Environ. Res. Public Health* **2018**, *15*, No. 414, DOI: 10.3390/ijerph15030414.
(25) Banipal, T. S.; Kaur, N.; Banipal, P. K. Binding Studies of Caffeine and Theophylline to Bovine Serum Albumin: Calorimetric and Spectroscopic Approach. *J. Mol. Liq.* **2016**, *223*, 1048−1055.
(26) Zhao, X.; Liu, R.; Chi, Z.; Teng, Y.; Qin, P. New Insights into the Behavior of Bovine Serum Albumin Adsorbed onto Carbon Nanotubes: Comprehensive Spectroscopic Studies. *J. Phys. Chem. B* **2010**, *114* (16), 5625−5631.
(27) Hu, Y.-J.; Ou-Yang, Y.; Dai, C.-M.; Liu, Y.; Xiao, X.-H. Binding of Berberine to Bovine Serum Albumin: Spectroscopic Approach. *Mol. Biol. Rep.* **2010**, *37* (8), 3827−3832.
(28) Ahmad, B.; Parveen, S.; Khan, R. H. Effect of Albumin Conformation on the Binding of Ciprofloxacin to Human Serum Albumin: A Novel Approach Directly Assigning Binding Site. *Biomacromolecules* **2006**, *7*, 1350−1356, DOI: 10.1021/BM050996B.
(29) Suryawanshi, V. D.; Walekar, L. S.; Gore, A. H.; Anbhule, P. V.; Kolekar, G. B. Spectroscopic Analysis on the Binding Interaction of Biologically Active Pyrimidine Derivative with Bovine Serum Albumin. *J. Pharm. Anal.* **2016**, *6* (1), 56−63.
(30) Il'ichev, Y. V.; Perry, J. L.; Simon, J. D. Interaction of Ochratoxin A with Human Serum Albumin. Preferential Binding of the Dianion and PH Effects. *J. Phys. Chem. B* **2001**, *106*, 452−459, DOI: 10.1021/JP012314U.
(31) Chen, T.; Zhu, S.; Shang, Y.; Ge, C.; Jiang, G. Binding of Dihydromyricetin to Human Hemoglobin: Fluorescence and Circular Dichroism Studies. *Spectrochim. Acta, Part A* **2012**, *93*, 125−130.
(32) Chin, S. F.; Pang, S. C.; Tay, S. H. Size Controlled Synthesis of Starch Nanoparticles by a Simple Nanoprecipitation Method. *Carbohydr. Polym.* **2011**, *86* (4), 1817−1819.
(33) Saharan, V.; Mehrotra, A.; Khatik, R.; Rawal, P.; Sharma, S. S.; Pal, A. Synthesis of Chitosan Based Nanoparticles and Their in Vitro Evaluation against Phytopathogenic Fungi. *Int. J. Biol. Macromol.* **2013**, *62*, 677−683.
(34) Salem, M. A. S.; Khan, A. M.; Manea, Y. K. A Novel Nano-Hybrid Carbon Architecture as Chemo Sensor for Natural Hazards: Active Adsorption of Rose Bengal Dye and Detection of Hazard Pollutants at Ppb Level. *J. Environ. Chem. Eng.* **2022**, *10* (1), No. 107032.
(35) Martins, J. G.; de Oliveira, A. C.; Garcia, P. S.; Kipper, M. J.; Martins, A. F. Durable Pectin/Chitosan Membranes with Self-Assembling, Water Resistance and Enhanced Mechanical Properties. *Carbohydr. Polym.* **2018**, *188*, 136−142.
(36) John, M. J.; Thomas, S. *Natural Polymers*; Royal Society of Chemistry, 2012.
(37) Qasem, K. M. A.; Khan, S.; Chinnam, S.; Saleh, H. A. M.; Mantasha, I.; Zeeshan, M.; Manea, Y. K.; Shahid, M. Sustainable Fabrication of Co-MOF@CNT Nano-Composite for Efficient Adsorption and Removal of Organic Dyes and Selective Sensing of Cr(VI) in Aqueous Phase. *Mater. Chem. Phys.* **2022**, *291*, No. 126748.
(38) Nabi, S. A.; Shahadat, M.; Bushra, R.; Oves, M.; Ahmed, F. Synthesis and Characterization of PolyanilineZr(IV)Sulphosalicylate Composite and Its Applications (1) Electrical Conductivity, and (2) Antimicrobial Activity Studies. *Chem. Eng. J.* **2011**, *173* (3), 706−714.

https://doi.org/10.1021/acsomega.3c04632
ACS Omega 2024, 9, 6339−6354

(39) Wang, Y.; Wang, X.; Li, L.; Gu, Z.; Yu, X. Controlled Drug Release from a Novel Drug Carrier of Calcium Polyphosphate/Chitosan/Aldehyde Alginate Scaffolds Containing Chitosan Microspheres. *RSC Adv.* **2014**, *4* (47), 24810−24815.
(40) Akram, M.; Anwar, S.; Bhat, I. A.; Kabir-ud-Din. Unraveling the Interaction of Hemoglobin with a Biocompatible and Cleavable Oxy-Diester-Functionalized Gemini Surfactant. *Int. J. Biol. Macromol.* **2017**, *96*, 474−484.
(41) Zaidi, N.; Ajmal, M. R.; Rabbani, G.; Ahmad, E.; Khan, R. H. A Comprehensive Insight into Binding of Hippuric Acid to Human Serum Albumin: A Study to Uncover Its Impaired Elimination through Hemodialysis. *PLoS One* **2013**, *8* (8), No. e71422.
(42) Naveenraj, S.; Anandan, S. Binding of Serum Albumins with Bioactive Substances - Nanoparticles to Drugs. *J. Photochem. Photobiol., C* **2013**, *14* (1), 53−71.
(43) Cao, X.-y.; Wang, S.; Tian, S.; Lou, H.; Kong, Y.; Yang, Z.; Liu, J. Spectroscopic and Molecular Modeling Studies on the Interactions of Fluoranthene with Bovine Hemoglobin. *Spectrochim. Acta, Part A* **2018**, *203*, 301−307.
(44) Anand, U.; Jash, C.; Boddepalli, R. K.; Shrivastava, A.; Mukherjee, S. Exploring the Mechanism of Fluorescence Quenching in Proteins Induced by Tetracycline. *J. Phys. Chem. B* **2011**, *115* (19), 6312−6320.
(45) Ross, P. D.; Subramanian, S. Thermodynamics of Protein Association Reactions: Forces Contributing to Stability. *Biochemistry* **1981**, *20* (11), 3096−3102.
(46) Bolattin, M. B.; Nandibewoor, S. T.; Joshi, S. D.; Dixit, S. R.; Chimatadar, S. A. Interaction between Carisoprodol and Bovine Serum Albumin and Effect of *β*-Cyclodextrin on Binding: Insights from Molecular Docking and Spectroscopic Techniques. *RSC Adv.* **2016**, *6* (68), 63463−63471.
(47) Alahdal, F. A. M.; Qashqoosh, M. T. A.; Manea, Y. K.; Mohammed, R. K. A.; Naqvi, S. Green Synthesis and Characterization of Copper Nanoparticles Using Phragmanthera Austroarabica Extract and Their Biological/Environmental Applications. *Sustainable Mater. Technol.* **2023**, *35*, No. e00540.
(48) Alahdal, F. A. M.; Qashqoosh, M. T. A.; Manea, Y. K.; Salem, M. A. S.; Khan, A. M. T.; Naqvi, S. Eco-Friendly Synthesis of Zinc Oxide Nanoparticles as Nanosensor, Nanocatalyst and Antioxidant Agent Using Leaf Extract of P. Austroarabica. *OpenNano* **2022**, *8*, No. 100067.
(49) Salem, M. A. S.; Khan, A. M.; Manea, Y. K.; Wani, A. A. Nano Chromium Embedded in F-CNT Supported CoBi-LDH Nanocomposites for Selective Adsorption of Pb2+and Hazardous Organic Dyes. *Chemosphere* **2022**, *289*, No. 133073.

https://doi.org/10.1021/acsomega.3c04632
ACS Omega 2024, 9, 6339−6354